Review of Scientific Instruments

Design of the ion-optics for the MRSt neutron spectrometer at the National Ignition Facility (NIF)

Cite as: Rev. Sci. Instrum. **93**, 033505 (2022); https://doi.org/10.1063/5.0080991
Submitted: 06 December 2021 • Accepted: 07 March 2022 • Published Online: 30 March 2022

G. P. A. Berg, J. A. Frenje, J. H. Kunimune, et al.

Review of Scientific Instruments ARTICLE scitation.org/journal/rsi

Design of the ion-optics for the MRSt neutron spectrometer at the National Ignition Facility (NIF)

Cite as: Rev. Sci. Instrum. 93, 033505 (2022); doi: 10.1063/5.0080991
Submitted: 6 December 2021 • Accepted: 7 March 2022 •
Published Online: 30 March 2022

G. P. A. Berg,[1,a)] J. A. Frenje,[2] J. H. Kunimune,[2] C. A. Trosseille,[3] M. Couder,[1] J. D. Kilkenny,[4] A. J. Mackinnon,[3] A. S. Moore,[3] C. S. Waltz,[3] and M. C. Wiescher[1]

AFFILIATIONS

[1] Department of Physics, Notre Dame College of Science, Notre Dame, Indiana 46556, USA
[2] Plasma Science and Fusion Center, Massachusetts Institute of Technology, Cambridge, Massachusetts 02139, USA
[3] Lawrence Livermore National Laboratory, Livermore, California 94550, USA
[4] General Atomics, San Diego, California 92186, USA

[a)] **Author to whom correspondence should be addressed:** gberg@nd.edu

ABSTRACT

A new Magnetic Recoil Spectrometer (MRSt) is designed to provide time-resolved measurements of the energy spectrum of neutrons emanating from an inertial confinement fusion implosion at the National Ignition Facility. At present, time integrated parameters are being measured using the existing magnet recoil and neutron time-of-flight spectrometers. The capability of high energy resolution of 2 keV and the extension to high time resolution of about 20 ps are expected to improve our understanding of conditions required for successful fusion experiments. The layout, ion-optics, and specifications of the MRSt will be presented.

I. INTRODUCTION

In order to achieve the planned ignition at the National Ignition Facility (NIF),[1] appropriate deuterium–tritium fuel distributions are required. At present, several time-of-flight spectrometers[2–4] and the Magnetic Recoil Spectrometer (MRS)[5–8] are used to measure the time-integrated energy spectrum of neutrons emitted from Inertial Confinement Fusion (ICF) experiments. These data allow for the determination[9] of the time-averaged burn parameters' areal density ρR, neutron yield Y_n, and ion temperature T_i in an ICF implosion. With the information obtained in these time-integrated measurements, it was possible to significantly improve ignition experiments.[10,11] In this article, we describe the ion-optical concept of a new spectrometer—MRSt[12]—that allows for time-resolved measurements of the neutron energy spectrum from which the evolution of an implosion can be deduced. This novel diagnostic technique will open a new window for ICF implosions. Section II describes the layout of the MRSt. Section III summarizes the design considerations and requirements, both given by the physics goals and the environment. Section IV gives a detailed presentation of the ion-optical design.

II. LAYOUT

The layout of the MRSt, shown in Fig. 1, is the result of an extensive design effort to fulfill and optimize all essential design parameters and requirements. The MRSt consists of two dipole magnets B1 and B2 bending in opposite directions with appropriate edge angles to provide focusing and two combined quadrupole and hexapole magnets Q1+Hex1 and Q2+Hex2 for adjustable focusing and hexapole corrections, respectively. The octupole OCT allows for third-order adjustments, i.e., mainly minimizing the curvature or sagitta of the focal plane (FP). A detailed discussion of the ion-optical concept and properties is given in Sec. IV.

The ion-optical part of the system starts at the deuterated foil positioned on the *Hohlraum* followed by a 5.8 m long drift to the adjustable entrance slit system that defines the solid angle. The entrance magnet Q1+Hex1 is followed by the two dipole magnets B1 and B2 with an octupole magnet OCT between them. The dipole magnets B1 and B2 provide the large momentum dispersion necessary for the high-energy resolving power. The focal plane downstream of the Q2+Hex2 is equipped with a Pulse-Dilation-Drift Tube (PDDT)[13] detector for the spatial and temporal measurements.

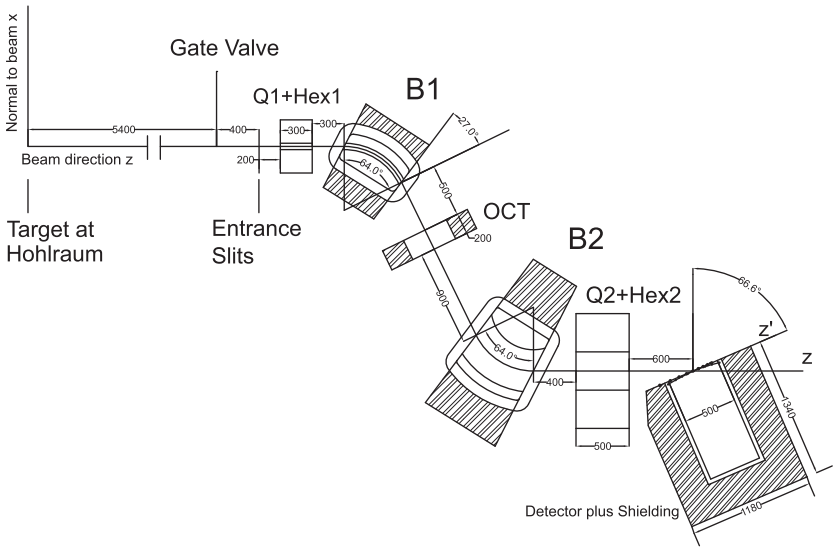

FIG. 1. Layout of the MRSt system in the dispersive plane. The annotations are defined in the text.

To allow for these measurements and corrections to some extent of the time differences (time skew) across the focal plane, the focal plane is tilted at an angle of 66.6° relative to the normal of the central ray. This angle is adjustable using Hex2 in the range from 0° to about 70°. The PDDT is surrounded by shielding consisting of a combination of Pb and polyethylene to reduce neutron background from the implosion and γ-ray background originating from (n, γ) reactions in the shielding.

III. DESIGN CONSIDERATIONS AND REQUIREMENTS

The goal is to provide time-resolved measurements of the ICF neutron energy spectrum. Therefore, a very high time resolution of the order of 20 ps in addition to a high ion-optical energy resolution of about 2 keV is required. This is achieved by first converting neutrons emanating from the implosion into deuterons in a deuterated foil at the *Hohlraum*.[14] The deuterons with energies in the range of 10.7–14.2 MeV will travel 5.8 m to and passing through the entrance slits positioned 0.2 m in front of the first magnet of the MRSt system that is mounted on the NIF target chamber.

The ion-optical calculations and optimizations were performed using the code COSY Infinity.[15,16] Conventions and definitions of this code are used throughout this article. The energy resolving power R_K of a focusing magnet system with $(x|a) = 0$ is defined by the energy dispersion $(x|\delta_K)$ divided by the magnification $(x|x)$ and half of the object size x_0 at the deuterated foil as follows:

$$R_K = \frac{(x|\delta_K)}{(x|x)x_0}, \tag{1}$$

where $\delta_K = (K - K_0)/K_0$ is the energy K relative to the central energy $K_0 = 12.45$ MeV.

This can be achieved by a system of two dipoles bending in either the same or opposite direction[17] with appropriated magnet settings to provide a high dispersion. We have studied both alternatives with similar results for energy and time resolutions. However, we present here the version with the dipole magnets bending in opposite directions since only this version can be accommodated on the NIF chamber without significant interference with existing equipment and support structures. The layout in the dispersive plane of the final design is shown in Fig. 1. The beam travels from the foil to the entrance slits. The curvilinear direction along the central ray is called the z direction. The x coordinate, normal to the z axis, is shown in the figure. The coordinate perpendicular, out of the z, x plane is the non-dispersive, y direction. A detailed discussion of the layout is given in Sec. II.

The following list summarizes the conditions and basic parameters that are required:

1. Acceptance of deuterons with energies of 12.45 MeV ± 14%.
2. An ion-optical energy and total time resolution of 2.0 keV and 20 ps, respectively.
3. Angle acceptances in the x and y directions sufficiently large to maximize efficiency without compromising the ion-optical energy and time resolutions.
4. Symmetrical focal plane image with a size smaller than 25 mm in the y direction.
5. An adjustable focal plane tilt angle in the range of 0° and about 70°.
6. Linear focal plane with deviations of less than 0.1 mm from linearity.
7. Higher order corrections up to order 3.
8. Accommodation at an available NIF chamber port with minimal interference with existing equipment.
9. Vacuum of better than 10^{-6} Torr, consistent with the vacuum in the NIF chamber.

The achieved first-order design parameters are listed in Table I. In normal operation, the focal plane tilt angle is 66.6° relative to the x direction. This is in agreement with the requirements of the focal plane detectors,[12] consisting of a front-end electron-producing cathode followed by a PDDT. The tilt angle is adjustable for fine tuning using the hexapole component Hex2 of the combined-function magnet Q2+Hex2. In addition, large angle changes are possible

TABLE I. Design parameters of the MRSt magnetic recoil spectrometer.

Focal plane tilt angle	deg	0	66.6
Deuteron energy	MeV	12.45	12.45
Energy acceptance	%	±14	±14
Energy resolution	keV	1.9	1.9
Time resolution, max. acceptance	ps	48	46
Time resolution, 50% acceptance	ps	32	32
Time resolution, 25% acceptance	ps	19	19
Focal plane length	m	0.135	0.341
Focal plane sagitta	mm	0.1	0.1
Angle acceptance a in the x direction	mrad	±0.1	±0.1
Angle acceptance b in the y direction	mrad	±1.0	±1.0
Image, y near the center of FP	mm	0.2	0.2
Image, y at both ends of FP	mm	6.3	23

using Hex2. For calibration purposes and comparison with the existing MRS time-integrating spectrometer, the system can operate with a focal plane tilt angle of 0°, i.e., perpendicular to the central ray. The design parameters in this mode are also listed in Table I. Note that the design parameters in Table I are for the central ray, unless otherwise noted. The parameters vary across the focal plane. In particular, the ion-optical energy and time resolutions vary across the focal plane. This will be discussed in more detail in Sec. IV.

The high time resolution of about 20 ps can only be achieved with a relatively small acceptance angle in the x direction. Ideally, the system should also be isochronous. However, in the present system, this is not possible and, therefore, a compromise was developed with limited acceptance angles a in the x direction and b in the y direction. As shown in Table I, at full angle acceptance a of ±0.1 mrad, the time resolving power is limited to 46 ps. To achieve a time resolution of 19 ps, the angle acceptance a has to be reduced by a factor of 4 as given in Table I. This is achieved by closing the entrance slits in the x direction. The time resolving power is less sensitive to opening of angle b in the y direction, which is opened to ±1.0 mrad to maximize the solid angle.

IV. OPTIMIZATION OF DESIGN

A. Ion-optical overview

One of the main challenges of developing the ion-optics for the MRSt was the simultaneous requirement of very high energy and time resolutions. Ideally, the time resolution requires an isochronous system, where the time-of-flight is constant within the energy and angle acceptances. While such systems can be designed,[18] the MRSt with limited space and a number of magnets does not have the flexibility to achieve isochronicity. The time resolution is particularly sensitive to the angle opening in the x plane due to the dispersion, compared to the y plane that does not have dispersion. Therefore, the MRSt has a relatively small angular acceptance of ±0.1 mrad in the x plane. In the y plane, the angular spread of ±1.0 mrad is much larger without contributing significantly to the time spread. With neutron yields expected $>10^{17}$ in near igniting targets, the count rate is sufficiently high, as discussed by Kunimune *et al.*[19]

After a drift of 5.8 m, the deuterons arrive at the entrance slits and enter the MRSt consisting of five magnets. The magnets are

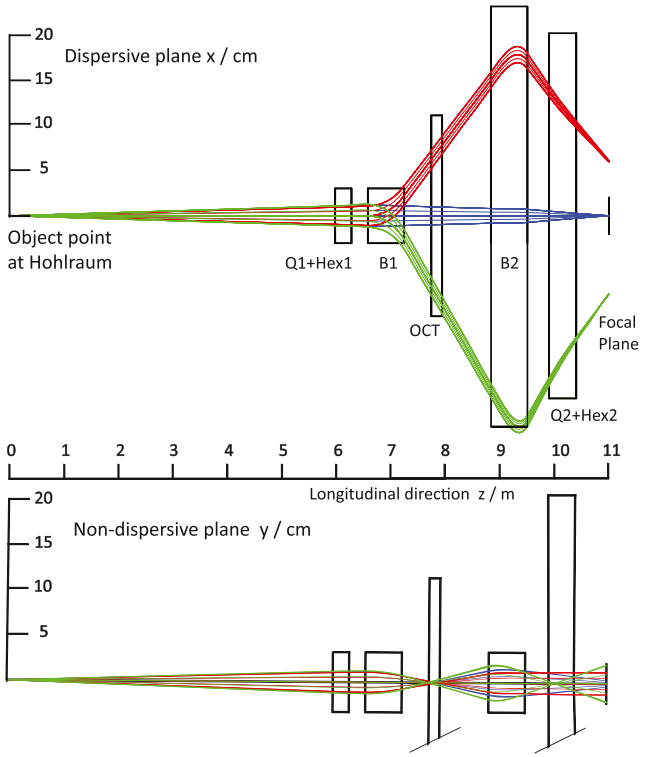

FIG. 2. Ion-optical design of the MRSt system. The rays are shown for three energies: the central energy of 12.45 MeV in blue, the lowest energy of 10.7 MeV in red, and the highest energy of 14.2 MeV in green. The annotations are defined in the text.

shown as rectangles where the size in the z direction is given by the effective-field length (EFL). In transverse x and y directions, the good-field regions (GFRs) of the magnets are shown. All rays fall within the GFR of the magnets ensuring full transmission. For the central energy, the system is focusing at the location marked focal plane. As shown in Fig. 1, the full focal plane is tilted relative to the normal. This is a second-order effect. This angle is adjustable in the range of 0° about 70° using the hexapole component of the Q2+Hex2 magnet as will be discussed in more detail below.

The ion-optical design is shown in Fig. 2. The calculation shown is of order 3. Higher order calculations up to order 7 were performed but are not affecting the performance significantly. The upper panel shows the optics in the dispersive x–z plane, and the lower panel shows the optics in the non-dispersive y–z plane. The longitudinal z direction is shown horizontally. The system is about 11 m long measured along the central ray starting with the object point, i.e., at the center of the deuterated foil positioned on the *Hohlraum*, where neutrons generate forward-scattered deuterons. These deuterons are analyzed in the MRSt magnet system with high energy and temporal resolutions as given in Table I. The object size is ±0.1 mm in the x direction and ±0.3 mm in the y direction. The angular acceptance is ±0.1 mrad in x and ±1.0 mrad in y. In Fig. 2 (upper panel), the rays shown span the angular range of ±1 mrad for illustration purposes, only. Therefore, the real spread of the rays are

TABLE II. Ion-optical transfer matrix elements of the MRSt.

Name of matrix element	Notation	
Spatial magnification in the x plane	$(x\|x)$	−0.365
Focusing in the x plane	$(x\|a)$	−0.004
Dispersion in the x plane	$(x\|\delta_K)$	0.474
⋯	$(a\|x)$	−0.424
Angular magnification in the x plane	$(a\|a)$	−2.743
Angular dispersion in the x plane	$(a\|\delta_K)$	−0.521
Spatial magnification in the y plane	$(y\|y)$	−0.139
Angular magnification in the y plane	$(b\|b)$	3.925
⋯	$(x\|a\delta_K)$	3.000
⋯	$(x\|a\delta_K\delta_K)$	2.881

ten times smaller than shown. The rays are shown for three energies, as explained in the figure caption.

The first-order transfer matrix elements listed in Table II define the ion-optical properties of the complete system from the object point to the FP. Higher order terms have been minimized and are negligible except for the second-order term $(x|a\delta_K)$ = 3.000 m/rad that defines the FP tilt angle Θ as per Eq. (2) and the third-order term $(x|a\delta_K\delta_K)$ = 2.881 m/rad that defines the FP radius R as per Eq. (3). The values given here are for a tilt angle of Θ = 67° and a radius of R > 1000 m, i.e., a straight FP. Changes in the tilt angle and optimization of the FP radius can be performed as explained in Secs. IV B and IV C, respectively.

B. Variable tilt angle

The tilt angle of the focal plane relative to the x direction can be adjusted for the particular detector system. In addition, fine adjustment of the angle may be necessary for a given detector system. We have included an adjustable hexapole component in the combined function Q2+Hex2. Figure 3 shows the tilt angle as a function of the Hex2 strength. The tilt angle is adjustable in the range from 0° to about 70°. This requires Hex2 pole tip strengths (at a radius of 20 cm) in the range from about 0 to 0.046 T. These adjustments also

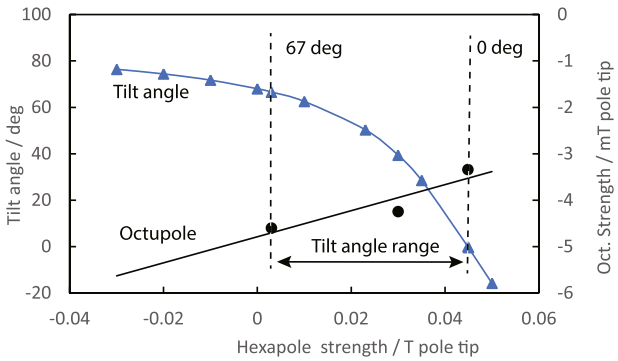

FIG. 3. The tilt angle as a function of Hex2 is represented by the blue calculated points and the blue curve to guide the eye. Also shown is the octupole strength represented by the black calculated points and the linear fit shown as a black solid line that is needed to keep the focal plane straight.

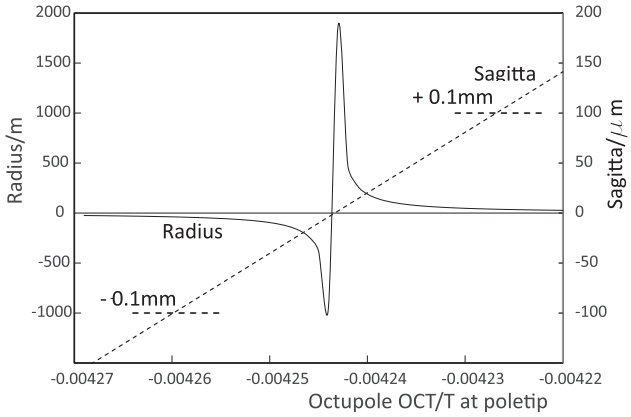

FIG. 4. Focal plane bend radius and sagitta as a function of OCT.

have an effect on the bend of the focal plane. The black solid line in Fig. 3 shows the octupole corrections in the range of −4.6 and −3.4 mT at the pole tip. The tilt angle Θ in degree is determined[17] by

$$\Theta = \text{atan}\left(\frac{-(x|a\delta_K)}{(a|a)(x|\delta_K)}\right)\cdot\frac{180}{\pi}. \tag{2}$$

C. Focal plane bending

As already mentioned, the focal plane may have a bend. This is a third-order aberration approximated by a radius R that is corrected for by a properly placed octupole. This radius is calculated[17] by

$$R = \frac{(x|\delta_K)^2}{(x|x)(x|a\delta_K\delta_K)}. \tag{3}$$

An example of the bend radius (solid line) for a tilt angle of 39° as a function of the variable octupole pole tip strength (at the radius of 11 cm) is shown in Fig. 4. In the figure, the sagitta (dotted line) is also shown. The dashed lines ±0.1 mm define the tolerance range of the octupole strength at the pole tip (−42.4 ± 0.2) Gauss. Note the focus in the non-dispersive plane (Fig. 2) at the location of the octupole OCT. This reduces third-order aberrations in this plane when adjusting OCT to minimize the sagitta.

D. Focal and isochronous plane

To illustrate the ion-optical properties of the MRSt in the detector plane x vs z, we show in Fig. 5 an enlargement of this region with rays (dotted arrow lines) of three energies. The focus of the central-energy ray (E = 12.45 MeV) is located at z = x = 0. The rays for the maximum and minimum energies are labeled and define the ends of the FP. The FP is linear because the sagitta has been minimized using the octupole OCT as explained in Sec. IV C. The locations of the y foci projected in the x–z plane, not shown in Fig. 5, are rotated relative to the FP plane creating a bowtie shape of the image in a position-sensitive detector placed along the FP. The effect of this is shown in Fig. 6 in the shape of the full y-size represented by blue squares and lines to guide the eye. The y-size is minimum at z′ = −0.05 m and has maxima at z′ = −0.28 and +0.14 m. Note that

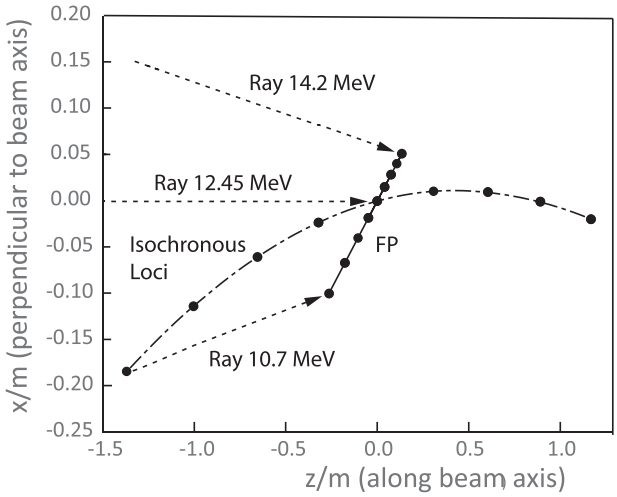

FIG. 5. Enlarged view of the focal plane region in the x–z plane.

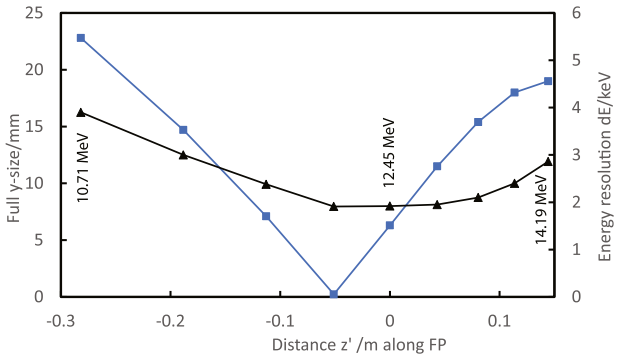

FIG. 6. The full size of the ray distribution in the vertical y direction and the energy resolution along the FP called the z′ axis.

the primed coordinates z′ are along the FP not to be confused with the ion-optical coordinate z. The y-extension of the beam has been optimized at the FP to minimize the y-size requirement of the FP detector. Figure 6 also shows the energy resolution along the FP. The energy resolution varies at 1.9 keV near the center of the FP and has its maximum of 3.4 keV at z′ = −0.28 m.

The ion-optical time resolution dt in units of ps is shown in Fig. 7 represented by blue squares for the full angular acceptances as defined in Table I. The ion-optical time resolution is defined as the time spread for a particular beam energy along the FP. The time spread is defined as a maximum time difference among 189 rays within the acceptances as defined in Ref. 20. It varies between 22 ps for z′ = 0.13 m and 75 ps at z′ = −0.26 m. If such a time resolution is not sufficient to time resolve the neutron energy spectra of a fusion burst with a typical length of 100 ps, it can be improved by closing the entrance slits in both the x and y directions, if the beam intensity is sufficiently high, e.g., by closing the slits by a factor of 2. For this case, the time resolution is shown in Fig. 7 as blue diamonds. It varies between 12 ps for z′ = 0.13 m and 30 ps at z′ = −0.26 m. The time

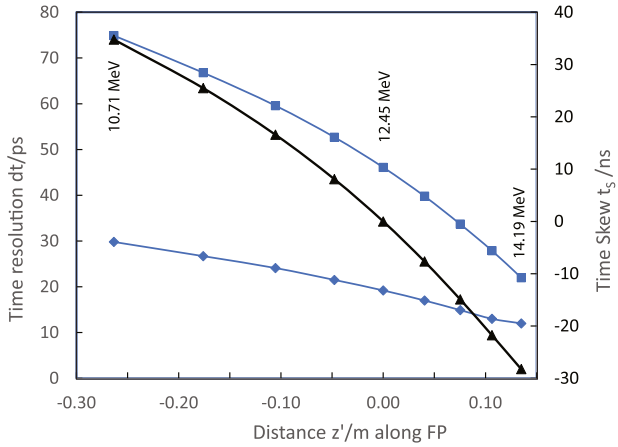

FIG. 7. The time difference, called time skew, between the isochronous loci and the FP along the FP called the z′ axis.

resolution, adjustable by the entrance slit openings, is a compromise between the high or low time resolution and the beam intensity.

The locations of the equal total flight times are shown as isochronous loci (dashed-dotted lines) in Fig. 5. In an ideal, isochronous system, these locations would coincide with the FP to avoid a large skew time t_s shown as a curve through black triangles in Fig. 7. This is the time-of-flight difference of a deuteron between the isochronous plane and the FP. However, for the given system, it was not possible to achieve this. Therefore, the time skew is about 35 ns at the FP location z = −0.27 m corresponding to the energy of 10.71 MeV and −29 ns at z′ = 0.14 m corresponding to the energy of 14.19 MeV.

An energy resolution of 1.9 keV ensures that the time spread due to the time skew does not contribute significantly to the time resolution.

V. CONCLUSION

We have developed a magnet system—MRSt—that allows us to measure the neutron spectra of a fusion implosion at the National Ignition Facility (NIF) with high ion-optical energy (2 keV) and temporal resolutions (20 ps). The system is designed with a pulse-dilation-drift tube detector in mind but is flexible enough to allow optimization and adjustment of the focal plane to accommodate other detector systems. In view of the recent improvement of the energy yield at NIF, this diagnostic is expected to identify early fusion inefficiencies and will hopefully help to increase the yield to and beyond ignition with appropriate remedies.

ACKNOWLEDGMENTS

This work was supported by the National Science Foundation under Grant Nos. PHY 08-22648 and PHY-1430152 (Joint Institute for Nuclear Astrophysics and JINA-CEE). Additional funds were provided by LLNL.

This work was performed under the auspices of the U.S. Department of Energy by Lawrence Livermore National Laboratory (Contract No. DE-AC52-07NA27344).

AUTHOR DECLARATIONS

Conflict of Interest

The authors have no conflicts to disclose.

DATA AVAILABILITY

The data that support the findings of this study are available within the article.

REFERENCES

[1]G. H. Miller, E. I. Moses, and C. R. Wuest, Nucl. Fusion **44**, S228 (2004).
[2]R. Hatarik, D. B. Sayre, J. A. Caggiano, T. Phillips, M. J. Eckart, E. J. Bond, C. Cerjan, G. P. Grim, E. P. Hartouni, J. P. Knauer *et al.*, J. Appl. Phys. **118**, 184502 (2015).
[3]M. G. Johnson, J. A. Frenje, D. T. Casey, C. K. Li, F. H. Séguin, R. Petrasso, R. Ashabranner, R. M. Bionta, D. L. Bleuel, E. J. Bond *et al.*, Rev. Sci. Instrum. **83**, 10D308 (2012).
[4]T. Clancy, J. Caggiano, J. McNaney, M. Eckart, M. Moran, V. Y. Glebov, J. Knauer, R. Hatarik, S. Friedrich, R. Zacharias *et al.*, Proc. SPIE **9211**, 92110A (2014).
[5]J. A. Frenje, K. M. Green, D. G. Hicks, C. K. Li, F. H. Séguin, R. D. Petrasso, T. C. Sangster, T. W. Phillips, V. Yu. Glebov, D. D. Meyerhofer *et al.*, Rev. Sci. Instrum. **72**, 854 (2001).
[6]J. A. Frenje, D. T. Casey, C. K. Li, J. R. Rygg, F. H. Séguin, R. D. Petrasso, V. Yu. Glebov, D. D. Meyerhofer, T. C. Sangster, S. Hatchett *et al.*, Rev. Sci. Instrum. **79**, 10E502 (2008).
[7]J. A. Frenje, D. T. Casey, C. K. Li, F. H. Séguin, R. D. Petrasso, V. Yu. Glebov, P. B. Radha, T. C. Sangster, D. D. Meyerhofer, S. P. Hatchett *et al.*, Phys. Plasmas **17**, 056311 (2010).
[8]D. T. Casey, J. A. Frenje, M. Gatu Johnson, F. H. Séguin, C. K. Li, R. D. Petrasso, V. Yu. Glebov, J. Katz, J. Magoon, D. D. Meyerhofer *et al.*, Rev. Sci. Instrum. **84**, 043506 (2013).
[9]J. A. Frenje, R. Bionta, E. J. Bond, J. A. Caggiano, D. T. Casey, C. Cerjan, J. Edwards, M. Eckart, D. N. Fittinghoff, S. Friedrich *et al.*, Nucl. Fusion **53**, 043014 (2013).
[10]D. T. Casey, J. L. Milovich, V. A. Smalyuk, D. S. Clark, H. F. Robey, A. Pak, A. G. MacPhee, K. L. Baker, C. R. Weber, T. Ma *et al.*, Phys. Rev. Lett. **115**, 105001 (2015).
[11]T. Ma, O. A. Hurricane, D. A. Callahan, M. A. Barrios, D. T. Casey, E. L. Dewald, T. R. Dittrich, T. Döppner, S. W. Haan, D. E. Hinkel *et al.*, Phys. Rev. Lett. **114**, 145004 (2015).
[12]J. A. Frenje, T. J. Hilsabeck, C. W. Wink, P. Bell, R. Bionta, C. Cerjan, M. Gatu Johnson, J. D. Kilkenny, C. K. Li, F. H. Séguin, and R. D. Petrasso, Rev. Sci. Instrum. **87**, 11D806 (2016).
[13]T. J. Hilsabeck, J. A. Frenje, J. D. Hares, and C. W. Wink, Rev. Sci. Instrum. **87**, 11D807 (2016).
[14]J. A. Frenje, Plasma Phys. Controlled Fusion **62**, 023001 (2020).
[15]K. Makino and M. Berz, Nucl. Instrum. Methods Phys. Res., Sect. A **427**, 338 (1999).
[16]M. Berz, COSY infinity, http://www.bt.pa.msu.edu/index_files/cosy.htm.
[17]W. Hermann, *Optics of Charged Particles* (Academic Press, Inc., Orlando, FL, 1987), ISBN: 0-12-762130-X.
[18]D. Bazin and W. Mittig, Nucl. Instrum. Methods Phys. Res., Sect. B **317**(Part B), 319 (2013).
[19]J. H. Kunimune, J. A. Frenje, G. P. A. Berg, C. A. Troisseille, R. C. Nora, C. S. Waltz, A. S. Moore, J. D. Kilkenny, and A. J. Mackinnon, Rev. Sci. Instrum. **92**, 033514 (2021).
[20]G. P. A. Berg, M. Couder, M. T. Moran, K. Smith, M. Wiescher, H. Schatz, U. Hager, C. Wrede, F. Montes, G. Perdikakis *et al.*, Nucl. Instrum. Methods Phys. Res., Sect. A **877**, 87 (2018).